

Article

The Growth and Evolution of Biomass Soot in Partial Oxidation-Assisted Hot Gas Filtration

Lin Tian ^{1,2,*} , Zixuan Jin ¹ and Wenran Gao ¹¹ New Energy Science and Engineering, Nanjing Forestry University, Nanjing 210037, China² Co-Innovation Center of Efficient Processing and Utilization of Forest Resources, Nanjing Forestry University, Nanjing 210037, China

* Correspondence: tianlinb0905101@foxmail.com

Abstract: At present, partial oxidation is applied in the filtration processes of biomass hot gas to aid in solving the blockage problems caused by tar and dust condensates. However, in the resulting high-temperature and oxygen-limited environment, the risk of tar polymerization forming soot is created during the purification processes. Thus, this work established a hardware-in-the-loop simulation model using the Lagrangian method coupled with the chemical reactions on the particle surface. The model was then used to simulate the entire evolution process of soot, including its formation, growth, and interception. The simulation results confirmed that under partial oxidation conditions, the increase in tar's conversion rate promotes the formation of soot. Further analysis indicated that the high-temperature field formed as a result of oxidation and the increase in the naphthalene/oxygen ratio are the main reasons for the soot formation. On the other hand, the growth process of soot was inhibited by partial oxidation, which is mainly reflected in the relatively smaller increasing magnitude of soot particle mass and the decrease in the soot formation rate. Although the formation and growth of biomass soot cannot be completely avoided, the growth process is beneficial to interception and the soot escape rate can be minimized by varying the premixed oxygen content. On this basis, the potential of the partial oxidation-assisted hot gas filtration method can be further investigated and analyzed.

Keywords: soot; partial oxidation; hot-gas filtration; discrete phase model

Citation: Tian, L.; Jin, Z.; Gao, W. The Growth and Evolution of Biomass Soot in Partial Oxidation-Assisted Hot Gas Filtration. *Energies* **2023**, *16*, 4233. <https://doi.org/10.3390/en16104233>

Academic Editors: Ana Ramos, Abel Rouboa and Eliseu Monteiro

Received: 31 January 2023

Revised: 17 May 2023

Accepted: 18 May 2023

Published: 21 May 2023



Copyright: © 2023 by the authors. Licensee MDPI, Basel, Switzerland. This article is an open access article distributed under the terms and conditions of the Creative Commons Attribution (CC BY) license (<https://creativecommons.org/licenses/by/4.0/>).

1. Introduction

The excessive consumption of conventional fossil-fuel-based energy resources has contributed largely to the global energy crisis and environmental problems, thereby forcing human beings to seek sustainable alternative energy resources. In this regard, biomass resources are abundant and can establish a regeneration cycle and carbon cycle through photosynthesis. Thus, their full utilization serves as a basis for an alternative and sustainable energy resource and a key player in carbon neutralization [1,2]. Moreover, pyrolysis or gasification are effective techniques for the utilization of biomass energy resources. The biomass gas (BAG) generated by pyrolysis or gasification has a wide range of applications, including direct use in boilers, internal combustion engines, and gas turbines to generate heat, produce electric power [3], and produce hydrogen gas. The hydrogen gas produced can be used as a fuel input for fuel cells and can even yield a variety of chemical products through chemical synthesis [4,5].

However, biomass raw gas contains impurities such as gaseous tar [6] and solid particulate matter [7,8]. Thus, dust and tar removal are needed to produce a gas that is suitable for long-distance transportation and can meet the cleaning standards required for combustion or chemical synthesis processes [9]. The particle size distribution of solid particulate matter in BAG is relatively wide, ranging from soot particles at the nanometer scale to dust at the micron scale. In this regard, most particulate matter can be removed through

inertial separation or filtration interception. Hot-gas filtration is a potential method that has been generally adopted in order to prevent the condensation of tar [10–12]. However, pulse back-blow is usually required to remove dust on the surface of the hot-gas filter. The resulting cooling effect will cause the tar to condense heterogeneously into solid particles as nuclei and solidify on the surface of hot-gas filter candles, causing blockage. For this reason, a partial oxidation method has been introduced as part of the hot-gas filtration processes to realize the separation of tar from dust through tar conversion. This can aid in effectively avoiding the blockage of tar-dust condensate.

The partially oxidation-assisted hot-gas filtration process leads to a high-temperature and oxygen-limited environment, in which tar undergoes two simultaneous competing reactions, namely cracking and polymerization. Cracking forms small-molecule hydrocarbons and non-hydrocarbon gaseous products. On the other hand, polymerization refers to the condensation growth of small-molecule aromatic rings through the hydrogen-abstraction–acetylene-addition mechanism (HACA) under high temperatures to form soot particles [13,14]. Thus, the introduction of oxygen not only realizes the oxidative elimination of soot [15–17], but also causes the formation of soot. On this basis, oxygen content is an important factor affecting the reaction process and controlling the resulting products. Previous studies indicated that the optimal conditions of the partial oxidation process are exhibited at a temperature of 400–600 °C, where hot gas is filtered under a low oxygen concentration of 0.5–1.5% in fuel gas. Under these conditions, the particles and the tar on the filter candles can be partially oxidized and the removal rate will reach its maximum [18]. As a parameter related to the oxygen content, the equivalent ratio (ER) also has an important effect and shall be optimized [19]. With the increase in the ER, the total amount of tar decreases rapidly. In this regard, an ER equal to 0.34 is a key value, allowing tar and soot to reach the minimum values of 0.26% and 4.07%, corresponding to the ER. Meanwhile, the dehydrocyclization of aromatic bases and the isomerization of polycyclic aromatic hydrocarbons also have a major impact on the formation of aromatic hydrocarbons. Reported research in the literature indicates that the hot-gas filtration process for BAG mainly undergoes an aromatization–condensation reaction accompanied by dehydrogenation and deoxidation under the oxygen-limited environment. As a result of these reactions, soot is formed easily. Moreover, in the partial oxidative environment (BAG + 2%O₂), the aromatization–polymerization reaction and the oxidation reaction can occur at the same time, and new surface-oxygen-containing groups will be generated through the oxidation reaction under the partial oxidative environment. This leads to the limitation of the polymerization of aromatic rings and thus a reduction in the generation of soot [20].

Furthermore, except for the oxygen content and ER, other factors such as the tar content in BAG, gas components, temperature, and pressure also have a major effect on the soot formation of partially oxidation-assisted hot-gas filtration. A study has verified that soot will no longer be produced when the tar (benzene) concentration is reduced below 0.2 vol% [21]. On the other hand, when the concentration is higher than 1 vol%, matter related to soot formation will appear, such as naphthalene. In addition, the effects of steam, hydrogen content, and CO₂ content in the gas on the formation of soot was found to be limited, while the methane content has a large impact on the soot formation. A study indicated that increasing the steam-to-methane ratio (S/C) can reduce the soot formation and increase the hydrogen output [16,22]. Further results also indicate that temperature plays a crucial role in increasing syngas production and reducing soot generation. Nevertheless, the pressure has an impractical impact on the syngas yield, leading to the formation of soot as well as a lower yield of hydrogen and carbon monoxide from BAG [16].

The review and discussion presented above highlight that many factors can affect the evolution of soot in the partial oxidation process of hot-gas filtration. This is primarily attributed to the complexity of the reaction process of hot-gas filtration; due to the introduction of oxygen, these complex reactions are interconnected and sometimes mutually restricted. In addition, multiple reactions' products will affect a series of processes such as the growth, extinction, filtration, and interception of soot. This will also affect the

conversion of tar, which in turn will have an impact on the composition of the gas and its calorific value. Therefore, it is necessary to investigate and examine the relationship between each reaction and the corresponding evolution of soot. To aid this, numerical simulation is a potentially attractive research method for predictions and assessment. This paper proposes a Lagrangian method to study the growth and evolution process of biomass soot in partial oxidation-assisted hot-gas filtration. The method will aid in the investigation and characterization of the relationship between tar conversion and soot generation. Furthermore, influencing factors on soot formation will be investigated, as will the reaction rules and interception characteristics of soot growth. The findings of this study are expected to set a basis for the optimal solid particulate matter and tar removal processes in partial oxidation-assisted hot gas filtration, with the aim of increasing the calorific value and controlling the optimized channel of soot growth and interception.

2. Models

2.1. Physical Models

In order to simulate the partial oxidization-assisted filtration process of the hot gas without experiencing purification and cooling in the fluidized bed, a filtering device physical model for biomass hot gas was established by simplifying the actual size of the test equipment, as shown in Figure 1. The test model inlet diameter was 0.2 m and the total length was 2.5 m, including a filter area length of 2 m. Considering the flow and interception characteristics of the mobile phase (hot gas) and the discrete phase (soot) through the filter pores, the filtering region was created by stacking solid rigid spheres. In order to enhance the calculation efficiency and simplify the calculations, the random variations in the pore structure of the porous media were neglected. Thus, the orderly stacking method was adopted. The stacked sphere had a radius of 4 cm, a staggered angle among interlayered particles, and a porosity of 53%. In addition, the filtering region used locally encrypted unstructured grids to obtain highly accurate simulation results, while the inlet and outlet transition regions used structured grids. These structured grids can make up for the slow operation of encrypted grids.

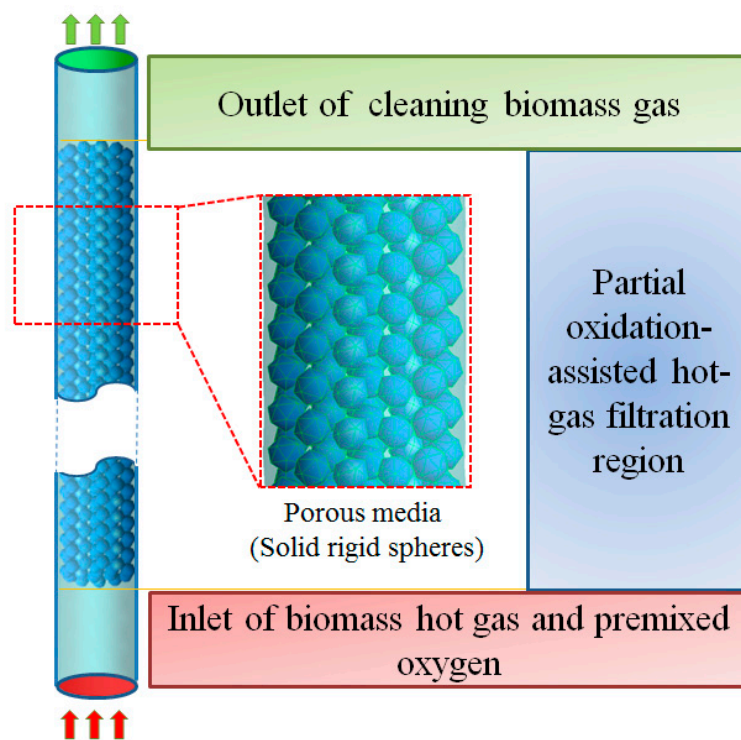


Figure 1. Physical model of the partial oxidation-assisted hot-gas filtration.

Furthermore, the establishment of control equations, including the equations of continuity, momentum, energy, and component, ensures the conservation of physical quantities in the region of the partial oxidation-assisted hot-gas filtration. The RNG κ - ϵ turbulence model was adopted in this work, and the discrete ordinates thermal radiation model was selected. The solution process implemented follows the uncoupled solution algorithm in order to solve the continuity, momentum, energy, and component transport equations in turn. In the solving process, the residual convergence criterion used for the energy equation was 1.0×10^{-6} , while 1.0×10^{-4} was used for the other equations.

2.2. DPM and Chemical Reaction Model

In this paper, the discrete phase model (DPM) of FLUENT, also known as the Lagrangian method, was adopted to simulate the behavior of the soot particles. The initial soot was made of carbon with a particle size of 5×10^{-8} m. Table 1 lists the chemical reaction models for the different reactions taking place on the particle's surface. This includes a series of chemical reactions, such as soot formation, oxidation, and the gasification of soot particles during partial oxidation-assisted hot-gas filtration. Each reaction process is controlled by the corresponding reaction kinetics parameters. The reaction rate K_r of each reaction can be expressed by the Arrhenius equation as:

$$K_r = A_r T^{\beta_r} e^{-E_r/RT} v_A^a v_B^b$$

Table 1. Chemical reaction models for surface reactions of the soot particles [23–26].

Number	Chemical Reaction	Reaction Type	A	β	E/(J·kmol ⁻¹)	a	b
R1	$C_6H_6 + 2H_2O \rightarrow 1.5C(s) + 2.5CH_4 + 2CO$	Polymerization of tar/formation of soot	$3.39 \times 1016 \cdot H^{-0.4}$	0	4.43×10^8	1.3	0.2
R2	$C_6H_5OH + 3H_2O \rightarrow 2CO + CO_2 + 2.95CH_4 + 0.05C(s) + 0.1H_2$		1×10^8	0	1×10^8	1	—
R3	$C_{10}H_8 \rightarrow 7.38C(s) + 0.275C_6H_6 + 0.97CH_4 + 1.235H_2$		$3.39 \times 1014 \cdot H^{-0.4}$	0	3.5×10^8	1.6	-0.5
R4	$2C(s) + O_2 \rightarrow 2CO$	Oxidation of soot	592-T	0	2×10^8	—	1
R5	$C(s) + H_2O \rightarrow CO + H_2$	Gasification of soot	3.6×10^{12}	0	3.1×10^8	1	1

A_r is the pre-exponential factor, β_r is the temperature index, E_r is the reaction activation energy, R is the gas constant, and a and b are the rate indexes of reactants A and B. In addition to the above gas–solid reaction between the soot particles and the gas, the partial oxidation-assisted hot-gas filtration also involves the oxidation reaction of the combustible components in the biomass hot gas, as shown in Table 2. In this study, toluene ($C_6H_5CH_3$), phenol (C_6H_5OH), benzene (C_6H_6), and polycyclic aromatic naphthalene ($C_{10}H_8$) were selected as the primary modeling compounds of tar. The four-component mixture is called full tar (hereinafter referred to as tar). Moreover, Table 3 lists the tar conversion reactions involved.

Table 2. Chemical reaction models for the oxidation of BAG [26–28].

Number	Chemical Reaction	A	β	E/(J·kmol ⁻¹)	a	b
R6	$2CO + O_2 \rightarrow 2CO_2$	$1.3 \times 10^{11} \cdot H_2O_{0.5}$	0	1.2567×10^8	1	0.5
R7	$2H_2 + O_2 \rightarrow 2H_2O$	1×10^{14}	0	4.2×10^7	1	1
R8	$CH_4 + 1.5O_2 \rightarrow CO + 2H_2O$	4.4×10^{12}	0	1.2552×10^8	0.5	1.25

Table 3. Chemical reaction models for the conversion reaction of tar [29–31].

Number	Chemical Reaction	A	β	E/(J·kmol ⁻¹)	a	b
R9	$C_6H_5CH_3 + H_2 \rightarrow CH_4 + C_6H_6$	3.3×10^{10}	0	2.5×10^8	1	0.5
R10	$2C_6H_5CH_3 + 21H_2O \rightarrow 7CO_2 + 29H_2 + 7CO$	2.323×10^{15}	0	3.56×10^8	1	0
R11	$C_6H_5CH_3 + 3.5O_2 \rightarrow 7CO + 4H_2$	3.8×10^7	0.5	5.545×10^7	1	1
R12	$C_6H_6 + 4.5O_2 \rightarrow 6CO + 3H_2O$	2.4×10^{11}	0	1.2552×10^8	-0.1	1.85

Table 3. Cont.

Number	Chemical Reaction	A	β	$E/(J \cdot kmol^{-1})$	a	b
R13	$C_6H_5OH + 4O_2 \rightarrow 6CO + 3H_2O$	$9.2 \times 10^6 \cdot T$	1	8×10^7	0.5	1
R14	$C_6H_5OH \rightarrow CO + 0.4C_{10}H_8 + 0.15C_6H_6 + 0.1CH_4 + 0.75H_2$	1×10^7	0	1×10^8	1	—
R15	$C_{10}H_8 + 7O_2 \rightarrow 10CO + 4H_2O$	$9.2 \times 10^6 \cdot T$	1	8×10^7	0.5	1

2.3. Semi-Physical Boundary Conditions

In order to ensure that the simulation results complied with the real processes and made sense from the scientific perspective, the hardware-in-the-loop model in this work was established. This means that the physical quantities measured in the physical test (calorific value of the inlet gas components, inlet oxygen content, inlet velocity, inlet temperature, inlet tar content, wall temperature, etc.) were imported as input boundary conditions for the developed model. In addition, the model was upgraded and calibrated by comparing the simulation data at the outlet with the real test data. The tuning was mainly performed by refining the boundary heat transfer conditions, such as the wall heat transfer coefficient and the temperature distribution characteristics of the wall and inlet. This ensures that the model had an acceptable accuracy and correctness.

2.4. Model Verification

As an important link in the model verification, an experimental study was carried out on the partial oxidation-assisted hot-gas filtration for BAG, as shown in Figure 2. The biomass gas containing tar and dust first entered the premixing device, where the oxygen premixed content was regulated. The mixed BAG then entered the bottom of the partial oxidation-assisted hot gas filtration. The temperature and pressure measurement points were distributed on the wall surface of the filter. The measurements were repeated 20 times to obtain accurate data. The specifications of the experimental device were consistent with the model information. The filtration velocity varied between 20 m/h and 40 m/h. The parameters of the inlet boundary conditions obtained by the hardware-in-the-loop method are shown in Table 4. The average value of the wall temperatures measured was taken as the input wall boundary temperature in the simulations. By comparison, the variation trends of the maximum simulation temperature and outlet gas calorific value with oxygen content were found to be consistent with the test results (Shown in Figure 3). This match between the two quantities verifies the correctness and accuracy of the simulation model.

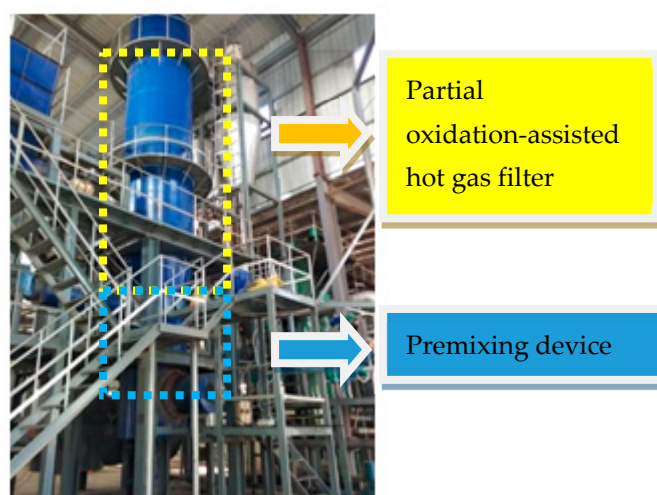
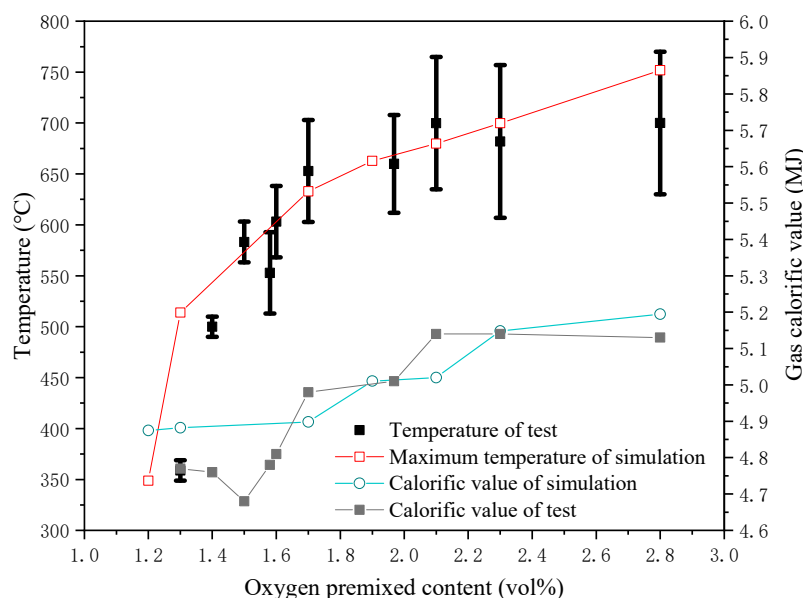


Figure 2. Equipment of the partial oxidation-assisted hot gas filtration process.

Table 4. Inlet boundary parameters.

Components and Caloric Value of Inlet Hot Gas	Caloric Value 4.9–5.1
Inlet oxygen content	1.2 vol%~2.8 vol%
Inlet initial temperature	400 °C
Inlet tar content	Total tar, accounting for 2.5 vol%–3 vol%

**Figure 3.** Experimental verification of the simulation results.

3. Results and Analysis

3.1. Tar Conversion and Soot Formation

Figure 4 shows the trajectory and mass distribution of the soot particles. It is shown that within the range of 0.1 m to 0.3 m from the inlet of the partial oxidation hot-gas filter, the mass of the soot particles increased rapidly and tended to be stable after reaching its peak value. On the other hand, the number of particles decreased gradually after the interception by the downstream filtering region, where a small amount of soot particles escaped away at the outlet. The rapid increase in the particle's mass indicated that soot was formed in the process of partial oxidation-assisted hot-gas filtration. At the same time, with the increase in the premixed oxygen content, the peak mass of the soot particles showed an increasing trend, and the location where the peak mass appears was much closer to the inlet. This was determined by the locations where the gas oxidation reaction occurred. Moreover, the formation of soot was closely related to the conversion of tar. Therefore, the tar's mass distribution cloud chart, shown in Figure 5, was analyzed under a premixed oxygen content of 2.3. It is shown that within a range of 0.4 m–0.5 m from the inlet, the formation region of soot, the tar's mass fraction showed a downward trend, and the conversion percentage also increased accordingly.

Although tar conversion is mainly completed by cracking and oxidation reactions, the reaction rate field diagram demonstrated that the polymerization of tar R1, R2, and R3 were relatively more active in the region. This was attributed to two main reasons. The first reason is related to the relatively high-temperature environment. It can be seen from the temperature field diagram presented in Figure 6 that a high-temperature area of 700–900 °C was formed within the range of 0.4–0.5 m. This is due to the homogeneous oxidation reactions R6, R7, and R8 between the premixed oxygen and the carbon monoxide and methane in the biomass hot gas. The heat generated led to the continuous rise in temperature in this region. In high-temperature environments, the reaction rates of R1, R2 and R3 (forming the soot) increased. Afterwards, the temperature dropped slowly due to the heat dissipation of the wall and the heat absorption of tar polymerization. The

second reason is the oxygen-limited environment. Since partial oxidation provides only a small amount of oxygen, the oxidation reaction of BAG led to a rapid reduction in the oxygen content within a high-temperature region, while the low-conversion percentage of tar led to the unconverted tar remaining in the region. Meanwhile, the tar's main components were transformed from phenol and toluene to benzene and polycyclic aromatic hydrocarbons (PAHs) such as naphthalene. This was primarily caused by the different conversion percentages corresponding to the different tar components. Furthermore, as shown in Figure 7, although the conversion percentage of full tar increased with the increase in the oxygen content, the conversion percentage of the phenol component accounted for the largest proportion of the total conversion, followed by toluene, and then benzene and naphthalene. As highlighted in Figure 8, under oxygen-limited conditions, the ratio between the mass fraction of naphthalene (as the precursor of soot) and the oxygen content increased sharply in the formation region of soot. In short, the rise in the temperature and the increasing naphthalene/oxygen ratio promoted the tar's polymerization, which led to the formation of soot.

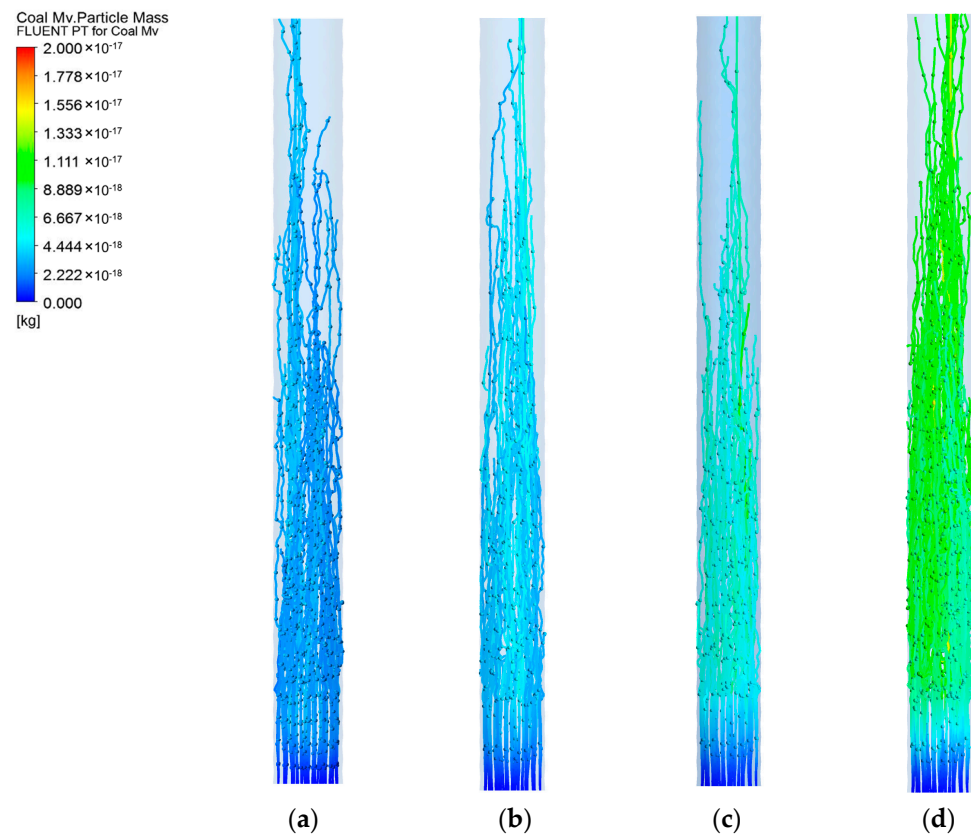


Figure 4. Mass fraction of soot particles with the increase in the premixed oxygen content. The premixed oxygen contents were: (a) 1.3 vol%; (b) 1.9 vol%; (c) 2.3 vol%; (d) 2.8 vol%.

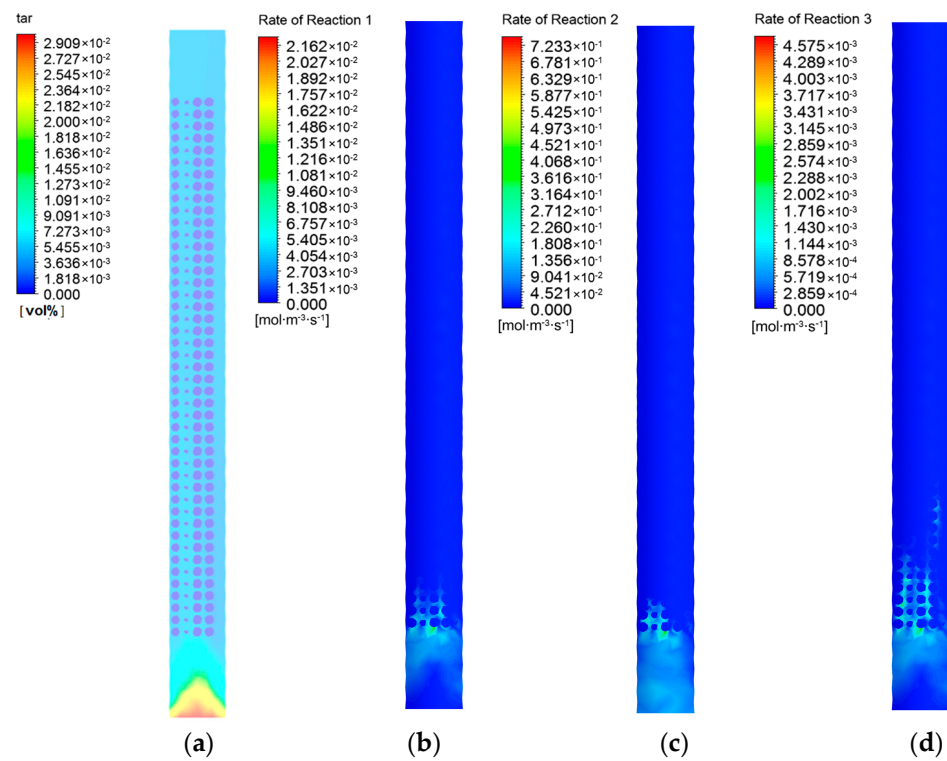


Figure 5. The mass distribution cloud chart of tar and the reaction rate fields of tar polymerization/soot formation. (a) Distribution of tar content; (b) Reaction R1; (c) Reaction R2; (d) Reaction R3.

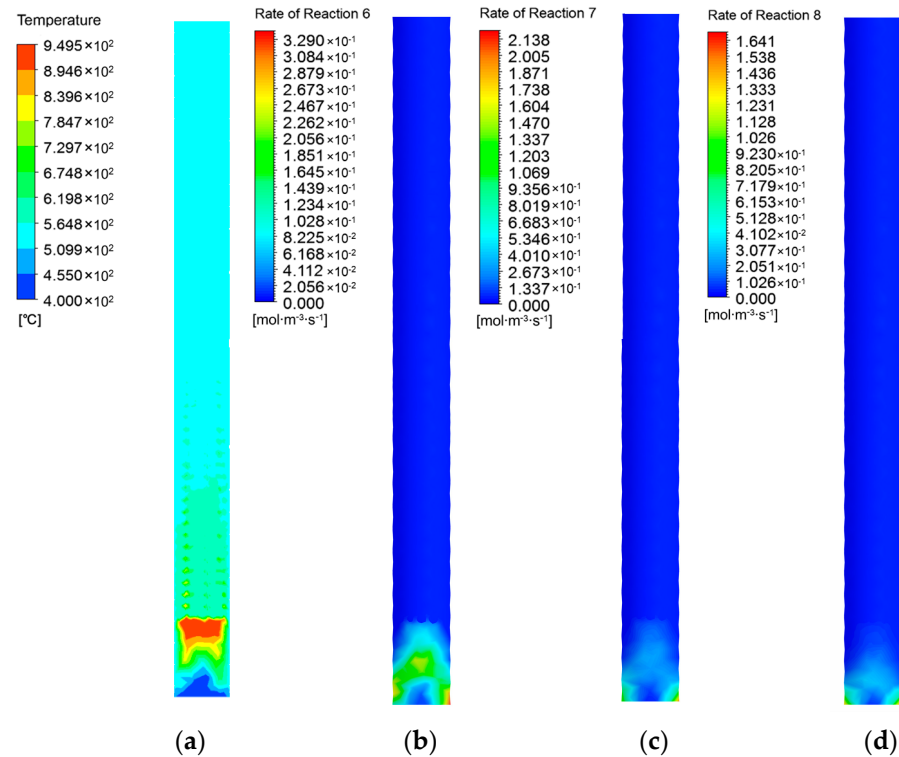


Figure 6. Temperature field and the gas component reaction rate field of partial oxidation-assisted hot-gas filtration. (a) Temperature field; (b) Reaction R6; (c) Reaction R7; (d) Reaction R8.

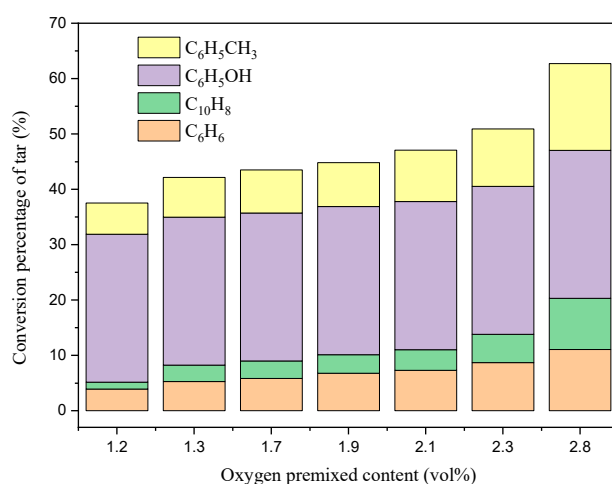


Figure 7. Conversion percentage of tar and the contribution weight of each component in the conversion.

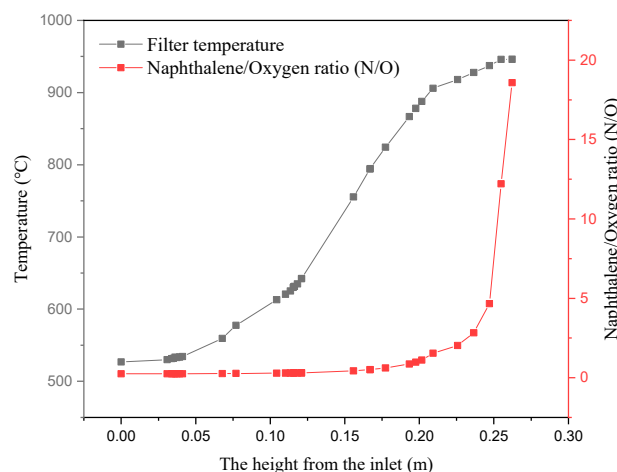


Figure 8. Temperature and naphthalene/oxygen ratio (N/O) variation trends in the filter.

3.2. Inhibition on Growth of Soot, Filtration, and Interception

In addition, after the soot particles are formed, the oxygen content was reduced to its lowest value. Meanwhile, the consumption reaction rate of soot by oxidation was lower than the formation rate of soot, leading to the growth of soot. Figure 9 shows the soot particles' mass distribution along the direction of the filter centerline. It is obvious that within the oxygen-limited range of partial oxidation the peak mass of the soot particle increased with the increase in the oxygen content. However, the enhancement of the tar's conversion percentage must increase the oxygen premixed content. This led to the unavoidable formation of soot in the partial oxidation-assisted hot-gas filtration process. Nevertheless, further results indicate that the introduction of oxygen inhibits the growth of soot. This is because the growth and evolution of soot are the result of the competition between the particle's oxidation consumption and tar's polymerization. It can be seen from the comparison results under two different conditions in Figure 9 that the increasing magnitude of the soot particle mass in the presence of the oxidation reaction R4 was significantly lower than that in the absence of this reaction. Additionally, Figure 9 showed that a premixed oxygen content below 1.3 vol% did not lead to the growth of soot. This is because the lower oxygen content results in a lower temperature, and thus the formation reaction of soot particles becomes weak. The mass of soot consumed by the oxidation reaction can be balanced by the amount of soot generated. The inhibitory effect on soot growth is not only reflected in the impact on the increase in soot mass, but also in the reduction in the formation rate of soot. Within the oxygen-limited range of partial oxidation,

Figure 10 indicates that the soot formation rates through the R1, R2, and R3 reactions were all significantly reduced in the presence of the R5 reaction, where the water required for the R5 reaction was generated by the BAG oxidation. In this regard, the reduction in the formation rate of soot resulting from that the H_2 and CO generated from R5 inhibited tar's polymerization. With the increase in the content of H_2 and CO, the reverse reaction rates of R1, R2, and R3 were aggravated, and thus the soot formation rates decreased. Furthermore, due to the increase in the H_2 content, the calorific value of BAG also increased.

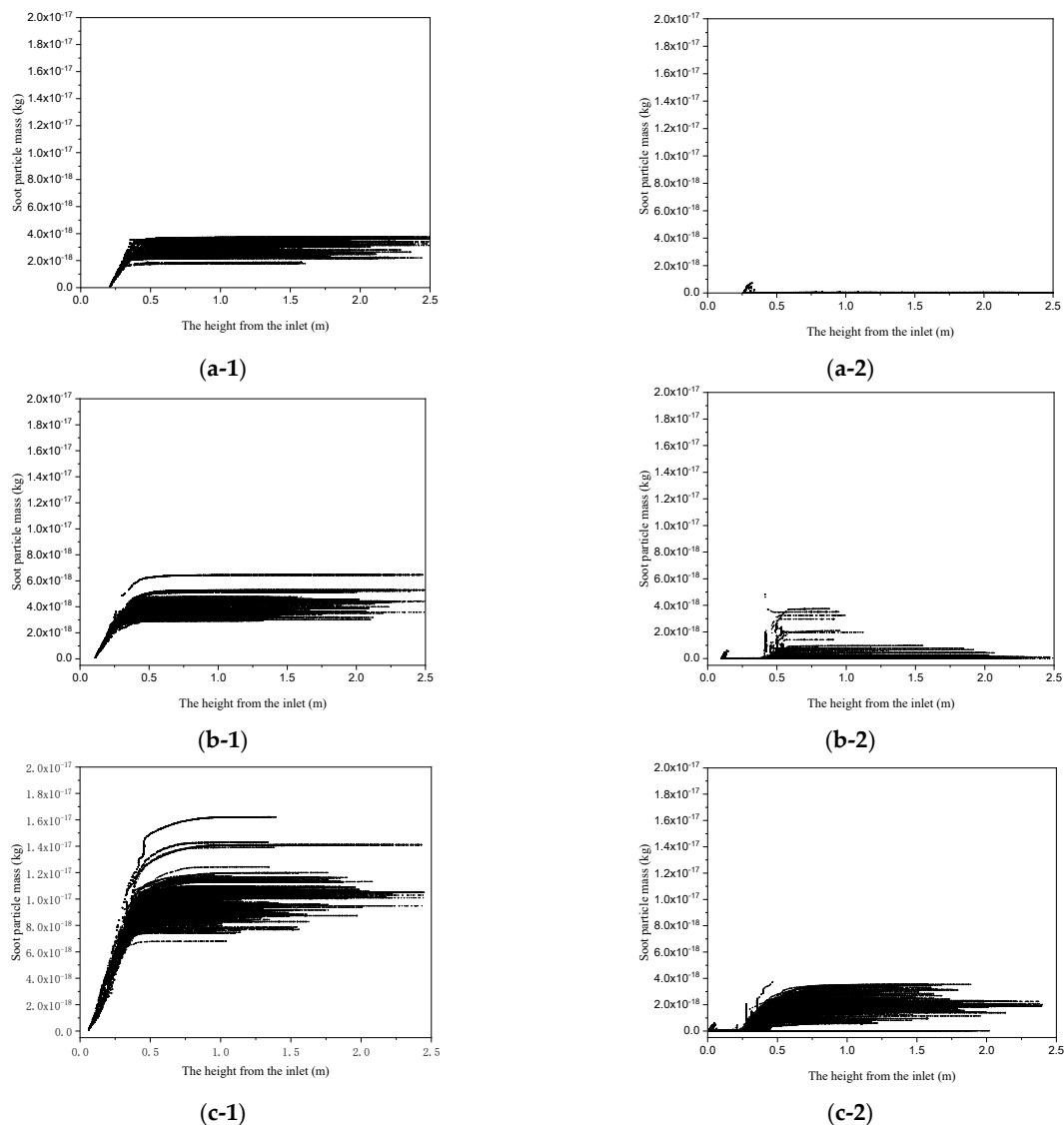


Figure 9. The inhibition of oxidation R4 on soot formation (soot particles' mass distribution along the direction of filter centerline). (a-1) In the absence of the reaction R4, the soot particle mass distribution when the oxygen premixed content is 1.3 vol%; (a-2) In the presence of the reaction R4, the soot particle mass distribution when the oxygen premixed content is 1.3 vol%; (b-1) In the absence of the reaction R4, soot particle mass distribution when the oxygen premixed content is 2.1 vol%; (b-2) In the presence of the reaction R4, soot particle mass distribution when the oxygen premixed content is 2.1 vol%; (c-1) In the absence of the reaction R4, soot particle mass distribution when the oxygen premixed content is 2.8 vol%; (c-2) In the presence of the reaction R4, soot particle mass distribution when the oxygen premixed content is 2.8 vol%.

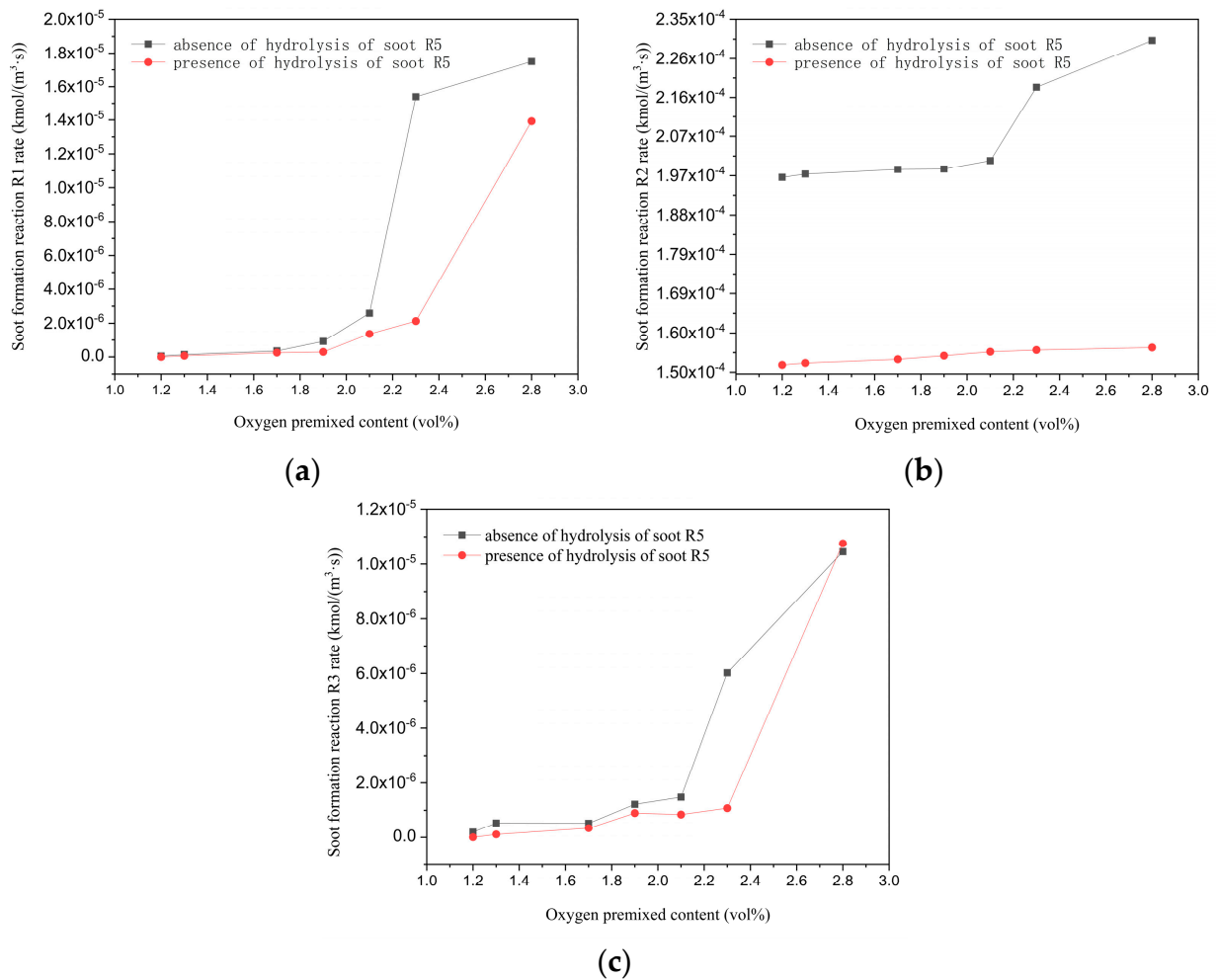


Figure 10. Inhibition of soot gasification reaction R5 on rate of the soot formation reactions R1, R2 and R3. (a) Reaction R1; (b) Reaction R2; (c) Reaction R3.

Although the mass of soot under a low oxygen content did not increase due to the inhibitory effect, the conversion percentage of tar was also very low. Thus, the interception of the soot particles formed needs to be considered. The interception effect can be evaluated by analyzing the outlet escape rate (the proportion of particles escaping among the total number of soot particles). The simulation results presented in Figure 11 show that, in the range of a low oxygen content 1.2 vol%–2.0 vol%, the soot escape rate decreased slightly with an increase in oxygen content. This indicates that the growth of soot particles was conducive to the interception in the filtering region. When the oxygen content continued to increase, the escape rate of soot showed an upward trend. The variation was due to the further increase in the number and mass of soot particles produced by the high oxygen content. It was noted that the formation and growth of soot in the hot gas filtration caused by partial oxidation could not be completely avoided. However, the presence of a low escape rate of soot can be used to expand the upper limit of premixed oxygen content and optimize the partial oxidation-assisted hot-gas filtration method.

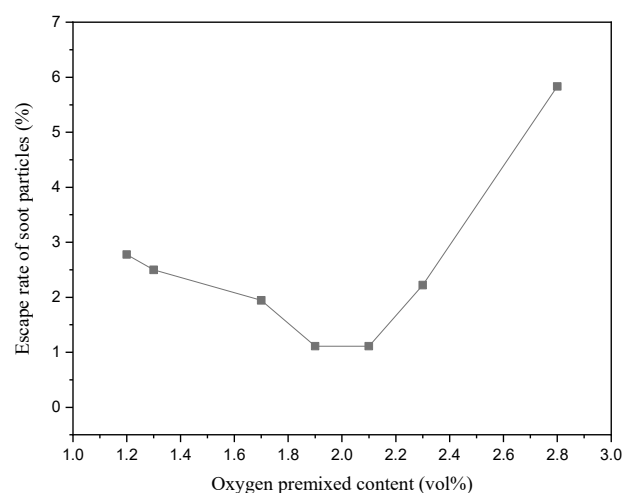


Figure 11. Variation of the escape rate of soot particles with the premixed oxygen content.

4. Conclusions

In this work, a DPM-coupled particle surface chemical reaction method was used to establish a hardware-in-the-loop model for simulating the generation, growth, oxidation, and interception of biomass soot particles in partial oxidation-assisted hot-gas filtration processes. The major findings of the study are as follows:

- (1) Although the partial oxidation method enhanced the conversion percentage of tar in the filtration process of biomass hot gas, the tar still generated soot through a polymerization reaction. This was mainly because the heat released by the gas oxidation reaction increased the temperature, and there was a higher naphthalene/oxygen ratio under oxygen-limited conditions.
- (2) Although the mass of soot particles increased with the increase in the oxygen content, the addition of oxygen inhibited the growth of soot particles. The inhibition was specifically embodied, with a lower increasing magnitude of the soot particle mass in the oxidation reaction and a reduction in the polymerization rate of tar due to the soot gasification reaction.
- (3) Partial oxidation led to the inevitable formation and growth of soot in the hot-gas filtration. Nevertheless, the presence of a low escape rate of soot provided a scientific basis to optimize the premixed oxygen content and further develop the application potential of partial oxidation-assisted hot-gas filtration.

Author Contributions: Conceptualization, L.T., Z.J. and W.G.; methodology, L.T.; software, Z.J.; validation, L.T. and W.G.; investigation, L.T.; writing—original draft preparation, L.T.; writing—review and editing, W.G. and Z.J.; visualization, L.T.; supervision, L.T.; project administration, L.T.; funding acquisition, L.T. and W.G. All authors have read and agreed to the published version of the manuscript.

Funding: This research was funded by the National Natural Science Foundation of China grant number (BK20200794).

Data Availability Statement: The data used in the study are available on request.

Acknowledgments: This work was supported by the National Natural Science Foundation of China (BK20200794).

Conflicts of Interest: The authors declare no conflict of interest. The funders had no role in the design of the study; in the collection, analyses, or interpretation of data; in the writing of the manuscript, or in the decision to publish the results.

References

1. Sansaniwal, S.K.; Rosen, M.A.; Tyagi, S.K. Global challenges in the sustainable development of biomass gasification: An overview. *Renew. Sustain. Energy Rev.* **2017**, *80*, 23–43. [[CrossRef](#)]
2. Díaz González, C.A.; Pacheco Sandoval, L. Sustainability aspects of biomass gasification systems for small power generation. *Renew. Sustain. Energy Rev.* **2020**, *134*, 110180. [[CrossRef](#)]
3. Situmorang, Y.A.; Zhao, Z.; Yoshida, A.; Abudula, A.; Guan, G. Small-scale biomass gasification systems for power generation (<200 kW class): A review. *Renew. Sustain. Energy Rev.* **2020**, *117*, 109486.
4. Singh Siwal, S.; Zhang, Q.; Sun, C.; Thakur, S.; Kumar Gupta, V.; Kumar Thakur, V. Energy production from steam gasification processes and parameters that contemplate in biomass gasifier—A review. *Bioresour. Technol.* **2020**, *297*, 122481. [[CrossRef](#)]
5. Shahabuddin, M.; Alam, M.T.; Krishna, B.B.; Bhaskar, T.; Perkins, G. A review on the production of renewable aviation fuels from the gasification of biomass and residual wastes. *Bioresour. Technol.* **2020**, *312*, 123596. [[CrossRef](#)]
6. Rakesh, N.; Dasappa, S. A critical assessment of tar generated during biomass gasification—Formation, evaluation, issues and mitigation strategies. *Renew. Sustain. Energy Rev.* **2018**, *91*, 1045–1064. [[CrossRef](#)]
7. He, Q.; Guo, Q.; Umeki, K.; Ding, L.; Wang, F.; Yu, G. Soot formation during biomass gasification: A critical review. *Renew. Sustain. Energy Rev.* **2021**, *139*, 110710. [[CrossRef](#)]
8. Feng, D.; Guo, D.; Shang, Q.; Zhao, Y.; Zhang, L.; Guo, X.; Cheng, J.; Chang, G.; Guo, Q.; Sun, S. Mechanism of biochar-gas-tar-soot formation during pyrolysis of different biomass feedstocks: Effect of inherent metal species. *Fuel* **2021**, *293*, 120409. [[CrossRef](#)]
9. Han, J.; Kim, H. The reduction and control technology of tar during biomass gasification/pyrolysis: An overview. *Renew. Sustain. Energy Rev.* **2008**, *12*, 397–416. [[CrossRef](#)]
10. Heidenreich, S. Hot gas filtration—A review. *Fuel* **2013**, *104*, 83–94. [[CrossRef](#)]
11. Li, S.; Baeyens, J.; Dewil, R.; Appels, L.; Zhang, H.; Deng, Y. Advances in rigid porous high temperature filters. *Renew. Sustain. Energy Rev.* **2021**, *139*, 110713. [[CrossRef](#)]
12. Andersson, K.J.; Skov-Skjøth Rasmussen, M.; Højlund Nielsen, P.E. Industrial-scale gas conditioning including Topsoe tar reforming and purification downstream biomass gasifiers: An overview and recent examples. *Fuel* **2017**, *203*, 1026–1030. [[CrossRef](#)]
13. Frenklach, M.; Clary, D.W.; Gardiner, W.C., Jr.; Stein, S.E. Detailed kinetic modeling of soot formation in shock-tube pyrolysis of acetylene. *Symp. (Int.) Combust.* **1985**, *20*, 887–901. [[CrossRef](#)]
14. Frenklach, M. Reaction mechanism of soot formation in flames. *Phys. Chem. Chem. Phys.* **2002**, *4*, 2028–2037. [[CrossRef](#)]
15. Stanmore, B.R.; Brillhac, J.F.; Gilot, P. The oxidation of soot: A review of experiments, mechanisms and models. *Carbon* **2001**, *39*, 2247–2268. [[CrossRef](#)]
16. Nourbakhsh, H.; Rahbar Shahrouzi, J.; Zamaniyan, A.; Ebrahimi, H.; Jafari Nasr, M.R. A thermodynamic analysis of biogas partial oxidation to synthesis gas with emphasis on soot formation. *Int. J. Hydrog. Energy* **2018**, *43*, 15703–15719. [[CrossRef](#)]
17. Josephson, A.J.; Gaffin, N.D.; Smith, S.T.; Fletcher, T.H.; Lignell, D.O. Modeling Soot Oxidation and Gasification with Bayesian Statistics. *Energy Fuels* **2017**, *31*, 11291–11303. [[CrossRef](#)]
18. Lang, L.; Yang, W.; Xie, J.; Yin, X.; Wu, C.; Lin, J.Y.S. Oxidative filtration for flyash & tar removal from 1.0 MWth fixed-bed biomass air gasification. *Biomass Bioenergy* **2019**, *122*, 145–155.
19. Su, Y.; Luo, Y.; Chen, Y.; Wu, W.; Zhang, Y. Experimental and numerical investigation of tar destruction under partial oxidation environment. *Fuel Process. Technol.* **2011**, *92*, 1513–1524. [[CrossRef](#)]
20. Na, L.; Lang, L.; Huacai, L. Isothermal partial oxidative pyrolysis mechanisms of solid particles from biomass gasification. *J. Fuel Chem. Technol.* **2018**, *46*, 290–297.
21. Valencia-López, A.M.; Bustamante, F.; Loukou, A.; Stelzner, B.; Trimis, D.; Frenklach, M.; Slavinskaya, N.A. Effect of benzene doping on soot precursors formation in non-premixed flames of producer gas (PG). *Combust. Flame* **2019**, *207*, 265–280. [[CrossRef](#)]
22. Svensson, H.; Tunå, P.; Hultberg, C.; Brandin, J. Modeling of soot formation during partial oxidation of producer gas. *Fuel* **2013**, *106*, 271–278. [[CrossRef](#)]
23. Ku, X.; Jin, H.; Lin, J. Comparison of gasification performances between raw and torrefied biomasses in an air-blown fluidized-bed gasifier. *Chem. Eng. Sci.* **2017**, *168*, 235–249. [[CrossRef](#)]
24. Gerun, L.; Paraschiv, M.; Vîjeu, R.; Bellettre, J.; Tazerout, M.; Gøbel, B.; Henriksen, U. Numerical investigation of the partial oxidation in a two-stage downdraft gasifier. *Fuel* **2008**, *87*, 1383–1393. [[CrossRef](#)]
25. Ismail, T.M.; Abd El-Salam, M.; Monteiro, E.; Rouboa, A. Fluid dynamics model on fluidized bed gasifier using agro-industrial biomass as fuel. *Waste Manag.* **2018**, *73*, 476–486. [[CrossRef](#)]
26. Loha, C.; Chattopadhyay, H.; Chatterjee, P.K. Three dimensional kinetic modeling of fluidized bed biomass gasification. *Chem. Eng. Sci.* **2014**, *109*, 53–64. [[CrossRef](#)]
27. Shin, D.; Choi, S. The combustion of simulated waste particles in a fixed bed. *Combust. Flame* **2000**, *121*, 167–180. [[CrossRef](#)]
28. Blasi, C.D. Dynamic behaviour of stratified downdraft gasifiers. *Chem. Eng. Sci.* **2000**, *55*, 2931–2944. [[CrossRef](#)]
29. Jeong, H.J.; Hwang, I.S.; Park, S.S.; Hwang, J. Investigation on co-gasification of coal and biomass in Shell gasifier by using a validated gasification model. *Fuel* **2017**, *196*, 371–377. [[CrossRef](#)]

30. Taralas, G.; Kontominas, M.G.; Kakatsios, X. Modeling the Thermal Destruction of Toluene (C₇H₈) as Tar-Related Species for Fuel Gas Cleanup. *Energy Fuels* **2003**, *17*, 329–337. [[CrossRef](#)]
31. Morf, P.; Hasler, P.; Nussbaumer, T. Mechanisms and kinetics of homogeneous secondary reactions of tar from continuous pyrolysis of wood chips. *Fuel* **2002**, *81*, 843–853. [[CrossRef](#)]

Disclaimer/Publisher’s Note: The statements, opinions and data contained in all publications are solely those of the individual author(s) and contributor(s) and not of MDPI and/or the editor(s). MDPI and/or the editor(s) disclaim responsibility for any injury to people or property resulting from any ideas, methods, instructions or products referred to in the content.